Flow decline during pore clogging by colloidal particles

N. Delouche,[1] B. Dersoir,[1] A. B. Schofield,[2] and H. Tabuteau[1,*]
[1]*Univ Rennes, CNRS, IPR (Institut de Physique de Rennes)-UMR 6251, F-35000 Rennes, France*
[2]*School of Physics and Astronomy, The University of Edinburgh, The James Clerk Maxwell Building, Peter Guthrie Tait Road, Edinburgh EH9 3FD, United Kingdom*

(Received 22 July 2021; accepted 14 March 2022; published 30 March 2022)

The flow of colloidal suspensions through porous media often leads to the deposition of particles inside the pores which increases the local hydrodynamic resistance by narrowing the pore space available and modifying the flow path of the transported particles. There is a significant flow decline in the extreme case when the entire porous medium becomes clogged. However, there are no experimental studies that determine directly the amplitude of this flow decline when compared with the dynamics of the formation of the particle deposit. This is mainly due to the great challenge of gaining experimental access to the features of the internal structure of the deposit as it grows and thus the ability to determine the flow inside it. In this paper, we show that is possible to monitor the flow decline corresponding to the successive deposition of colloidal particles inside a constriction (pore), ending by its complete blocking. The variation of the flow is determined by the measurement of the velocity of the particles through our channel. Such a technique coupled to the precise knowledge of what is deposited inside the pore, thanks to image analysis, enables us to determine the different contributions to the flow decline. We also use numerical simulations to access the flow inside the porous structure of the deposit as it grows. Together, experiments and simulations demonstrate that the obstruction process and the subsequent limited growth of the clog, corresponding to a few layers of accumulated particles, have a higher impact on the amplitude of the flow decline than the extra growth of the clog.

DOI: 10.1103/PhysRevFluids.7.034304

I. INTRODUCTION

Most of us have experienced the decline in flow associated with the clogging of kitchen and bathroom strainer sinks. As pieces of food, hairs, or other types of small debris are transported by water towards the grid that composes the strainer they start to accumulate and the flow rate suddenly decreases. This flow decline also occurs in many other situations when suspensions of smaller particles, i.e., colloidal particles, flow through porous structure like filters [1], nozzles of inkjet printers [2], irrigation drippers [3], microfluidic devices [4], chemical reactors [5,6], soils [7,8], and fractured rocks [9], where they can also be coupled to seismic events [10,11]. The permeability reduction of a porous media due to particle deposition is highly dependent on the stability and the size of the colloidal suspension and can reach three orders of magnitude with nanoparticles [12–14]. However, from these previous works we cannot determine the relative contribution to the flow decline at the pore or the particle scales, since the pores are interconnected. Indeed, we do not know to what extent the progressive fouling of adjacent pores is coupled. In addition, we cannot follow the capture or deposition of colloidal particles over time inside these pores in order to monitor

*herve.tabuteau@univ-rennes1.fr

the growth of the clog. Microfluidic experiments with transparent model porous media, coupled with various imaging techniques, have provided important information on the dynamics of the clog formation in such conditions. Some of these experiments helped define for which pore geometries [15,16], degree of confinement [4,15–19], and flow [4,15,16] pore clogging occurs, while others focused on the geometrical features and size of particles that compose the clog [20–23]. Only a few studies have simultaneously monitored the dynamics of clog growth and the variation of the flow conditions [4,24]. Sauret *et al.* performed clogging experiments with a single pore and have determined the permeability of a forming clog after it was well developed, knowing the volume of the clog and the particle volume fraction, and using the Carman-Kozeny relationship [24]. With their measurements they were unable to capture the strong variation of the permeability at the very beginning of the clogging process, when the pore cross section is first completely blocked. They supposed that the permeability of the clog head is high and does not contribute significantly to the hydrodynamic resistance of clog as it grows. Thus, up to now, nobody has measured the flow decline associated with the early moment of the clog formation. This partly comes from the fact that such measurements require simultaneous imaging of the deposition of particles that compose the forming clog and monitoring of the flow variations inside the pore. While the former experimental constraint can be easily met by using high frame rates [15,16] the latter is really challenging since there is no flow sensor accurate and fast enough to measure such important brief flow variations at the pore scale. It would be beneficial to perform such measurements to detect the early stage of clog formation as this information may be used to prevent their subsequent growth. This is particularly important in industrial filtration operations where the amplitude of the flow decline directly impacts the stoppage of the filtration process by giving information about when the filter should be cleaned or replaced [25].

In this paper we describe the clogging transition in a single pore by imaging the forming clog and tracking the colloidal particles transported by the fluid through the pore. This enables us to determine the variation of the flow conditions and the nature and type of particles that compose the clog. We consider the influence of the confinement and the composition of the colloidal suspensions. We also perform numerical simulations of the flow within a forming clog and inside one that has stopped growing to better understand the flow variations corresponding to the clogging transition. We show that three consecutive phenomena contribute to the flow decline associated with the clogging transition. First, there is a sharp flow decline due to the progressive narrowing of the cross section of the pore (channel), up to its complete obstruction. The magnitude of this first flow decline increases when the particle size used to construct the clog decreases as the mean pore size between the particles is smaller. After this initial obstruction event, the subsequent accumulation of a few layers of particles causes the average fluid velocity to decrease significantly as some of the remaining preferential flow paths through the clog are progressively closed. This closure process forces the fluid to flow on average through narrower pores which increases the hydrodynamic resistance of the clog. Finally, further growth of the clog leads to the smallest contribution to the flow decline, even for long clogs, and the fluid velocity is proportional to the inverse of the clog length, a characteristic of Darcy's flow.

II. MATERIALS AND METHODS

The soft lithography methodology used to make our model microfluidic filter and their geometrical features are identical to those of used in Delouche *et al.* [21,22]. Briefly, we design model filters with either one pore or several independent pores. In both cases the particles first flow through a reservoir before entering a narrow zone (dimensions $20\,\mu\text{m} \times 20\,\mu\text{m} \times 310\,\mu\text{m}$) in front of the constriction itself. This constriction has a square cross section with a height and width of $8\,\mu\text{m}$ and it is $120\,\mu\text{m}$ long. It is here that the clog initially forms and the channel blocks. See Fig. 1.

The two reservoirs are long enough to perform particle tracking and obtain the particles' velocity using a sensitive camera (Hamamatsu Orca Flash 4.0 v2). We also used a similar model filter for confocal imaging and this had a rectangular cross section with the width and height of the pore

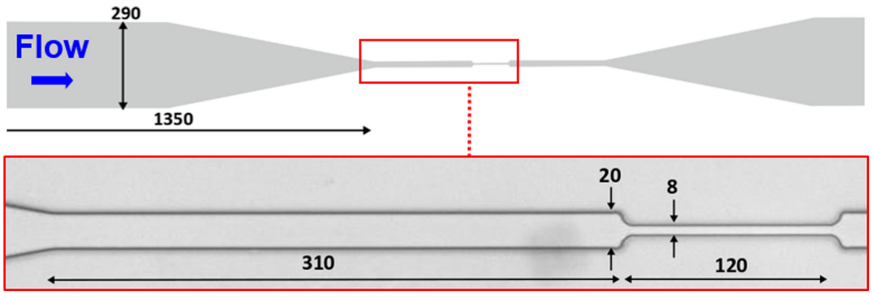

FIG. 1. Geometrical features of the single-channel experiment. All dimensions are in microns. The channel is generally clogged in its narrowest part and the particle velocities are determined in the long reservoir zone just upstream of this.

being 9 and 11 μm, respectively. We bond the Polydimethylsiloxane (PDMS) channel on a glass slide covered by a thin layer of PDMS to ensure that particle-surface colloidal interactions are identical everywhere on the pore surface. The suspension is injected in the filter by applying a difference of pressure with a regular pressure controller (Elveflow OB1 Mk2 or Fluigent MSFC). A flow sensor (Fluigent, 5% accuracy) is used to determine the corresponding flow rates at the beginning of the experiments. Fluid inertia is negligible with Reynolds numbers for the different flow conditions always smaller than 10^{-3}. We used either home-synthesized fluorescent Polymethyl methacrylate (PMMA) particles with a 1.8-μm diameter and stabilized by a polymer brush [21] or 1.6- and 3-μm Polystyrene (PS) particles with sulfate groups at their surface bought, respectively, from Thermofisher (Life, USA) and Microparticles GmbH (Germany). We used different aqueous mixture to obtain isodense suspension to negate particle sedimentation inside the channel. The distributions of particle size and particle type, single particles or aggregates of various sizes, for each suspension are determined during "stop and go" experiments [22]. Such experiments allow us to see that there is 6.7×10^{-3}% of large particles in the 1.6-μm PS suspension. The particle size and -type distributions of the 1.8-μm PMMA are provided in Delouche *et al.* [21].

The flow decline corresponds to successive particle depositions within the pore zone. The deposition of particles leads to an increase of the hydrodynamic resistance of the channel, and since we work with a fixed pressure there is a flow rate decline and a decline in the particle velocity. Unfortunately, regular methods like flow meters or the weighing of the liquid that flows out of the filter are not able to provide accurate measurements of such small variations of the flow conditions. To circumvent this issue we decided to perform *in silico* measurements of the flow rate variation thanks to the velocity of the particles. In our flow conditions, with low Reynolds number smaller than 10^{-3} and Péclet number between 4×10^5 and 1.8×10^4, particles follow fluid streamlines and act as flow tracers.

We are able to track all the particles that flow through the pore with a moderate frame rate of 100 frames per second. The determination of the particles velocity is made in the reservoir, upstream of the pore, thanks to particle tracking. We also capture the deposition of particles inside the pore by image analysis. We calculate the average particle velocity from the instantaneous velocity of 100–2000 particles, depending on the particle type, prior to the pore completely blocking while we use only 30–50 particles after the pore clogging with a particle volume fraction of the feeding suspension equal to 5×10^{-4}. In this latter condition, since we average over a lower number of particles, we also have a lower precision on the average particles' velocities. The variation of the imposed pressure, which is about 0.2 mbar, also induces an uncertainty in the particles' velocity. These two effects taken together lead to an error in the particle velocity of 10 μm/s. We determine the flow conditions inside the channel more or less filled with particles thanks to finite-element software (COMSOL). For the clog formed with 3-μm PS particles we used the positions of the particles inside the clog as determined by bright-field microscopy. We have a precision of 0.4 μm

for the particle center in the *XY* plane, i.e., along the flow direction. We are also able to determine the approximate position of the particles along the height of the channel due to the high confinement of the 3-μm particles within the pore's 8-μm $\times$ 8-μm cross section. Indeed, there are only two to three particle layers along this height, a particle being either close to the top or the bottom horizontal surface or somewhere near the middle. We end up with a maximum of 1 μm for the particle center along the channel height. For the clog formed with 1.8-μm PMMA particles we used confocal microscopy to obtain a more accurate 3D location of the particle centers with a precision of 50 nm. For the 3-μm PS and the 1.8-μm PMMA particles we determine the flow condition each time a new particle deposits in the channel, using the steady-state Navier-Stokes model. No-slip boundary conditions are applied on the channel walls. We also impose the same pressure gradient used in the experiments and we take into account that the fluid viscosity is slightly higher than the water viscosity. We determine the flow rate over the entire clogging process in the same cross section, located downstream of the particle accumulation, and then calculate the corresponding mean velocity of the fluid in this section. We perform the same kind of simulation for the 1.8-μm PMMA particles but we add ten particles at a time instead of just one before determining the flow conditions across the clog

III. RESULTS

A. Flow decline measurements

We first look at the general features of the flow decline during the clogging of a single pore with various types of colloidal suspensions. The variation of the flow decline over time is rather similar irrespective of the type of suspension and can be separated into three stages (Fig. 2). There is first a sharp decline of the flow corresponding to complete obstruction. The shape of the flow decline curve in this step is highly dependent on the way the first particles pile up and clog the pore, i.e., particles can be identical [Fig. 2(a)], be a mixture of aggregates and single particles [Fig. 2(c)], or a mixture of big and small particles [Figs. 2(d) and 2(e)], all these examples corresponding to most of the common cases seen in real-world pore clogging. In the highest confinement, for the 3-μm particles, the progressive narrowing of the pore relies massively on the particles captured by at least one wall of the pore, and thus depends mainly on the Derjaguin-Landau-Verwey-Overbeek (DLVO) particle–pore-wall interactions. For the 1.8-μm PMMA colloids, spherical particles are first deposited onto the pore surfaces, which then helps in capturing several aggregates and this is enough to obstruct the pore and allow sieving of spherical particles [20,21]. During the pore narrowing some edges of the aggregates are in contact with the surfaces of the pore while other edges can be in contact with the particles already deposited. Therefore, the stability of the growing deposits and the clog for 1.8-μm PMMA relies on both DLVO interactions among particles and between particles (aggregates) and the pore surfaces. For 1.6-μm PS the pore is mainly blocked by either a big particle, followed by the sieving of smaller particles [Fig. 2(d)], or the successive deposition of particles and small aggregates before a big particle joins the deposit [Fig. 2(e)]. Only in this latter case are interparticle and particle-surface DLVO interactions responsible of the cohesion of the deposits (clog). As in the case of the 1.8-μm PMMA particles, aggregates are mainly responsible for the pore clogging for the 1.6-μm PS particles since these spherical particles also cannot form multilayers. In a second stage there is a limited accumulation of particles in the clog over a length, L_{clog} between 10 and 20 μm, corresponding to 1.2–2.5W and this depends on the composition of suspension and the way the clog is formed, in particular the length along the pore over which the deposits grows before it eventually clogs the pore. Even though this limited accumulation corresponds to a couple of layers of particles along the pore it has an important contribution to the flow decline. Finally, in the third step, the flow keeps decreasing but much less rapidly, with the particle accumulation and the temporal evolution of the flow almost identical for different trials with the same suspension [Fig. 3(a)]. During this step the velocity decrease is inversely proportional to L_{clog} [Fig. 3(b)], consistent with Darcy's law. For a given suspension and a fixed clog length, the corresponding amplitude of the overall flow

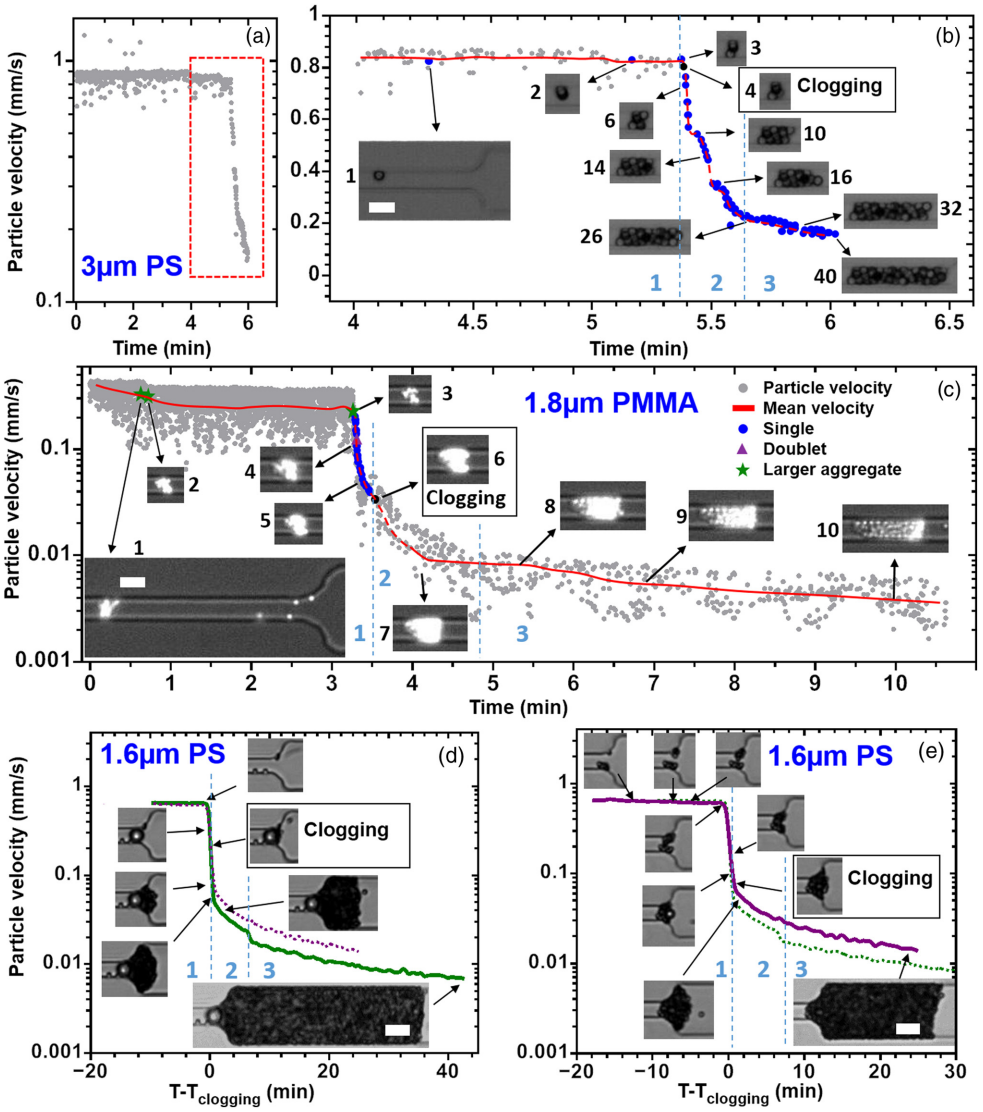

FIG. 2. (a) Instantaneous velocity of all the 3-μm particles flowing towards the pore with an applied pressure of 7 mbar. (b) Close-up on the clogging transition (dashed rectangle in the left graph). Blue dots correspond to the events of particle deposition while the continuous and dashed lines are, respectively, the average particle velocity and a guide to the eyes. The dark dot corresponds to the last particle that effectively blocks the pore. For each image we give the number of particles that compose the clog at that moment. (c) Variation of the instantaneous particle velocity for 1.8-μm particles over time, with the same definition for the symbols, the continuous and dashed lines. The applied pressure is equal to 3 mbar. The first four images labeled with a number correspond to the deposition of an aggregate. The term "large aggregate" means that the aggregate is composed of at least three particles. Nineteen individual particles are captured where the clog is formed in addition to a doublet and three large aggregates. (d), (e) Evolution of the mean particle velocity for the 1.6-μm particle suspension also composed of few larger particles. The applied pressure is equal to 3 mbar. For each graph the images are related to the continuous line. The dotted line in the left corner graph is the continuous line used in the right corner graph and vice versa. All the scale bars correspond to 10 μm and the image of the complete obstruction of the pore is outlined by a black rectangle. The three stages of the flow decline are separated by two vertical dashed lines in (b) to (e).

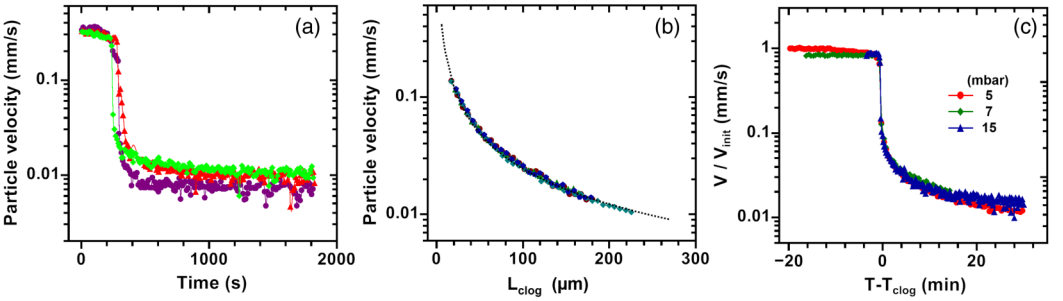

FIG. 3. (a) Particle velocity decline over time during three clogging experiments with 1.8-μm PMMA particles for an applied pressure of 15 mbar. (b) Variation of the velocity of 2-μm PS particles that accumulate at the rear of the clog with the L_{clog} for an applied pressure of 8 mbar and in the same pore geometry. The dotted line is a fit of the data indicating that the particle velocity is inversely proportional to the length of the clog. (c) Variation of the velocity of 2-μm PS particles scaled by their initial velocity prior to particle deposition in the constriction with time for various applied pressure. At $T - T_{\text{clog}} = 0$ the pore is completely obstructed.

decline is almost constant [Figs. 2(d) and 2(e)], which is also the case when we change the applied pressure of the feeding suspension [Fig. 3(c)].We observe a substantial increase of this amplitude when we use feeding suspensions composed of smaller particles (Fig. 2).

Note that the timescale of the clogging process is mainly fixed by the particle volume fraction of the suspension, i.e., the higher the particle concentration the faster the clogging process is for a given pore [22]. From all these observations we conclude that most of the flow decline corresponds to the blocking of the pore and the early stages of the clog growth while further accumulation of particles only leads to a small decrease of the flow conditions. In order to understand why there is such a sharp flow decline over the first tens of microns of the clog we use numerical simulations of the flow within the forming clog.

B. Numerical simulation of the flow in the forming clog

We perform flow simulation within the forming clog using COMSOL to determine the flow variations each time a new particle is added to the clog. We use the approximate positions of the particles inside the pore obtained from the images of the deposited 3-μm PS particle whose velocity decline over time is shown in Fig. 2(b). We progressively form the clog, from the first deposited particles up to the end of the accumulation process where the clog is composed of 40 particles and is about 30 μm long. Here, we do not want to faithfully reproduce the flow conditions encountered in the experiment but rather study the flow inside a realistically structured clog. However, we check that slightly changing the position of the particles inside the clog, especially during the complete obstruction of the pore by the first four particles, does not significantly modify the flow decline. Once we add a new particle at the rear of the clog we determine the flow velocity across the entire clog (Fig. 4) and also velocity map its porous structure, in several cross sections (Fig. 5). A comparison between the numerical and experimental data is provided in Fig. 6. The overall shape of the fluid velocity decline across the clog as particles deposit inside the pore in the numerical simulation is similar to that of the particles' velocity in the experiment. However, the velocity decline for the fluid is much greater than that of the particles, in particular for the complete pore obstruction by the first four particles (Fig. 6). The particle velocity is reduced by only 4, while that of the fluid is reduced by 30 on the overall accumulation. This difference comes from the fact that very few particles are used, sometime only one, to calculate the mean particle velocity in the experiment between each particle deposition event. The finite size of the particles is also responsible for the difference in the decline amplitude. Indeed, 3-μm particles cannot move along streamlines close to the wall of the pore, and on average over a cross section they are going faster than the fluid.

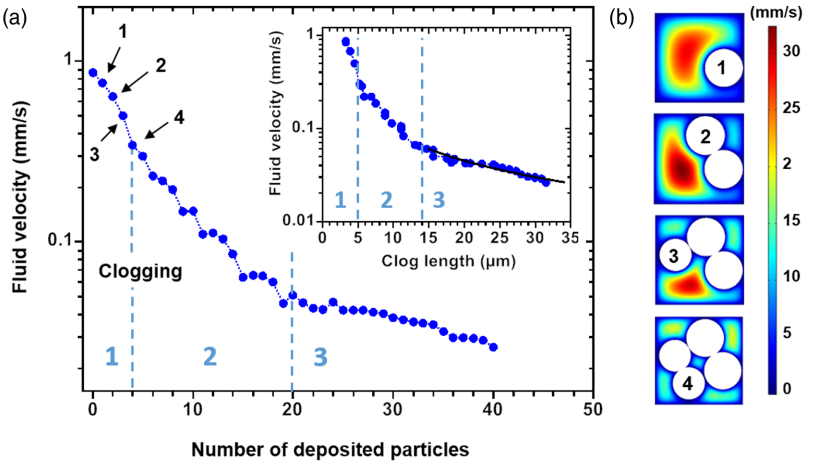

FIG. 4. (a) Variation of the average fluid velocity through the clog as particles accumulate in a numerical simulation of the clog formation and the flow within it. The average fluid velocity in the pore without any particle inside corresponds to the first point of the graph. The pore is clogged when four particles successively deposit, the end of the process being outlined by the vertical dashed line. (Inset) Evolution of the fluid velocity with the clog length. The dotted lines correspond to the deposition of the 20th particle from which the fluid velocity varies as the inverse of L_{clog} (continuous line). The three stages that contribute to the flow decline are separated by two dashed lines. (b) Velocity map in the first clogged cross section of the channel by the successive deposition of four particles, labeled with their arrival number.

The evolution of the flow decline in the numerical simulation can also be separated into three consecutive steps. There is first a sharp decrease of the velocity when the pore is completely obstructed by the successive deposition of four particles [Fig. 4(b)].

This step corresponds to an important reduction of the cross section available for the flow, since the fluid has to pass through five pores between the particles and the channel surfaces at the end of the complete obstruction of the pore [Fig. 4(b)]. Later on, 16 particles accumulate, adding 3–4 particles layers at the rear of the clog whose total length is equal to 8–9 μm. This very limited growth of the clog leads to an even more important flow decline than the pore narrowing. Finally, the addition of another 20 particles at the rear of the clog results in the half reduction of Q, each particle deposition only slightly modifying the flow rate. In this last part of the flow decline, the fluid velocity decreases as the inverse of the clog length, indicating that there is a Darcy flow across the clog, suggesting that the permeability of the clog is constant on average [Fig. 4(a), inset]. We can conclude that most of the flow decline takes place over a clog length equal to the width of the pore.

The evolution of the flow decline once the pore is blocked by the deposition of the first four particles can be understood by looking at the flow distribution within the forming clog (Fig. 7). As new particles accumulate, we hypothesize that a few flow paths that connect both ends of the clog are created with most of the fluid flowing through these preferential channels since they have a lower hydrodynamic resistance than the other narrower paths. However, at the same time the accumulation of a particle may also block one of these paths or modify their tortuosity, resulting in an increase of the local hydrodynamic resistance and also in a partial redistribution of the flow. To illustrate this process we consider the variation of mean fluid velocity at the head of the clog, inside the first blocked cross section when new particles accumulate. The fluid flows through five pores in this cross section, four of them being in the corners while the last one is in the middle [Fig. 5(b), inset]. We suppose that if low preferential flow paths persist and connect both ends of the clog as particles accumulate then the flow will leave the clog head via one of these pores. As expected, each

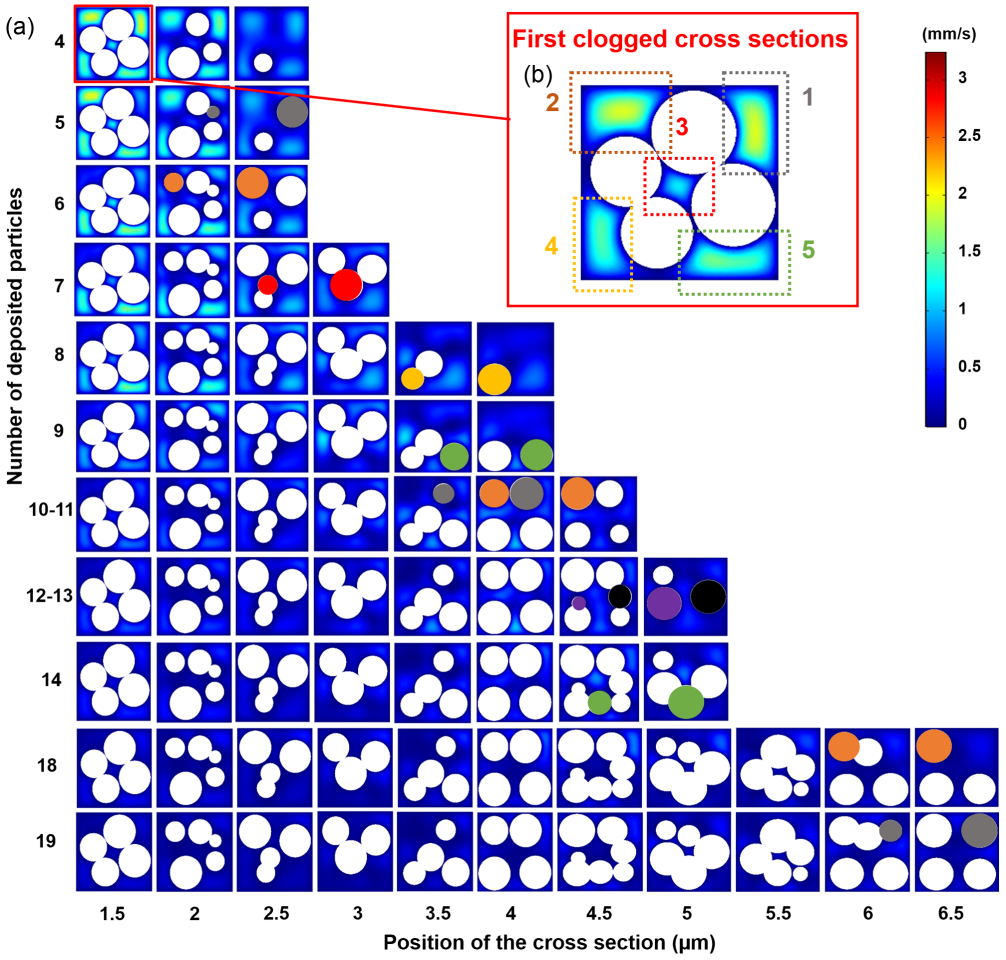

FIG. 5. (a) Evolution of the flow velocity inside various cross sections (columns) of the entire clog for the deposition of the first 19 particles that compose the clog. Each line corresponds to the deposition of one or two particles. (b) Close-up of the first cross section of the pore clogged by four particles. The five dotted rectangles outline the pores between the particles through which the fluid has to flow in the first clogged cross section (first line and first column). We give the same color to a pore and the particles that directly modify the flow condition in this pore when they deposit, i.e., particles No. 5, No. 10, and No. 19 are in gray and induce a flow decline in the pore number in (a). The 12th and the 13th particles have different colors to show that they do not contribute directly to the flow decline of any pore of the first cross section.

time a particle deposits and blocks more or less one of the five preferential flow paths the velocity decreases in the corresponding pore identified in this first blocked cross section (Fig. 5, first seven lines). Only a part of the flow upstream of the blocking particle will follow the initial flow path, up to the clog head, while the other parts of the flow will be redirected in other directions [26] (Fig. 5, line 4 to 9). Once around 20 particles accumulate, the fluid velocity is about the same in each cross section along the channel, meaning that there is no preferential flow path anymore at this stage of the clog formation (Fig. 5, line 19).

To be more quantitative, we monitor the variations of the fluid velocity inside the pores belonging to four cross sections along the clog as particles pile up (Fig. 7). As long as the number of particles that compose the clog is lower than 14–18, the flow inside the clog is rather heterogeneous with

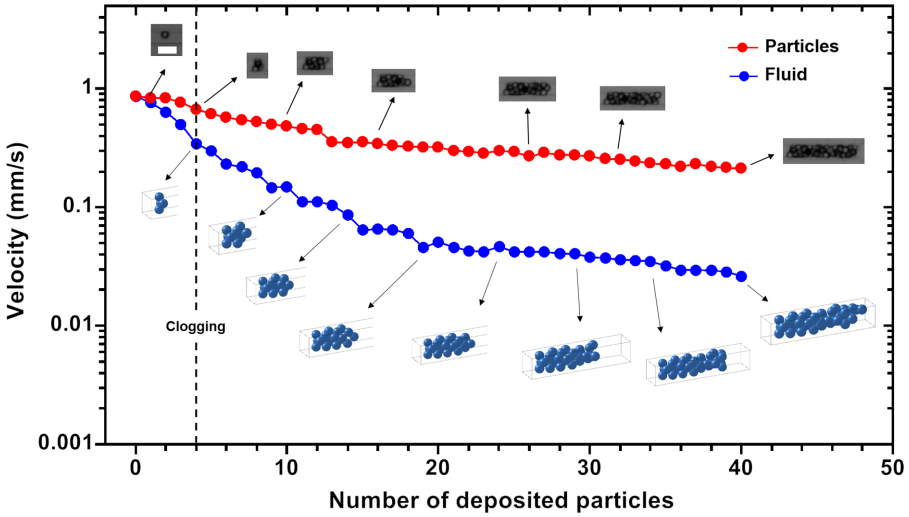

FIG. 6. Variation of the particle velocity and the fluid velocity with the number of deposited particles, respectively, from the experiments and the numerical simulations. The experimental data are those used in Fig. 2(b). There is no deposited particle inside the pore for the first point of the two curves, which gives us the same value for both velocities. We also provided images or 3D views of the accumulation as the clog grows from the simulations and bright-field images from the experiment. The scale bar corresponds to 10 μm.

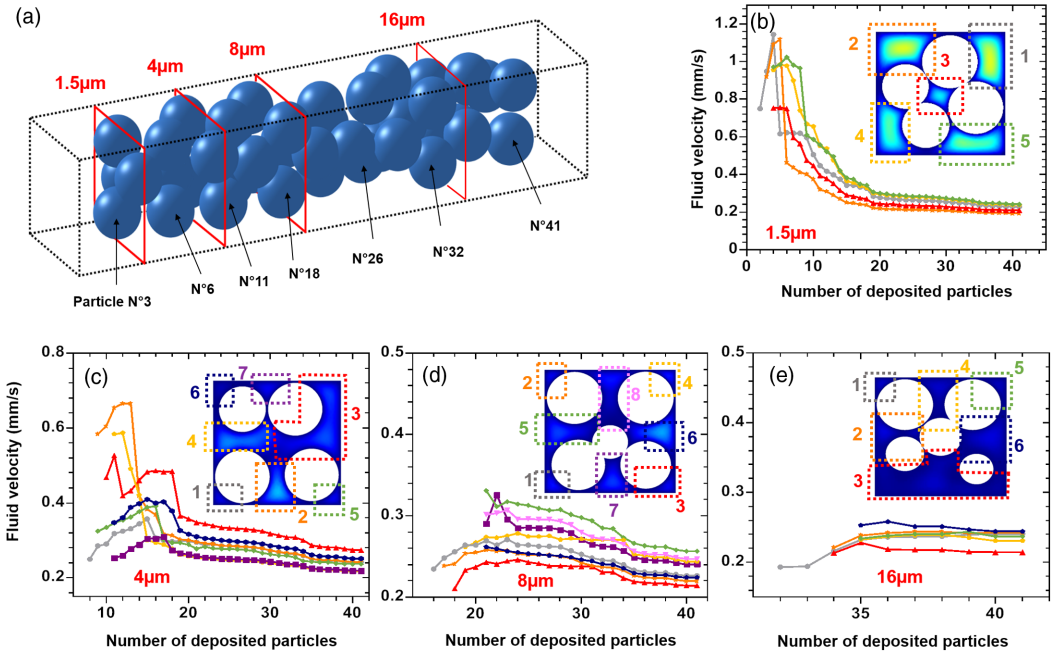

FIG. 7. (a) Three-dimensional representation of a clog composed of 41 particles with a diameter 3 μm in a COMSOL simulation. The position of four slices used in the other parts of this figure [(b)–(d)] are outlined. For each of these slices, located at 1.5 μm (b), 4 μm (c), 8 μm (d), and 16 μm (e) from the clog head, we determine the variation of velocity within its pores as particles accumulate at the rear of the slice. We use the same colors in the image of each slice to outline the pores and the variation of the fluid velocity inside them as depicted in the graphs.

the fluid velocity being different in each pore of the different cross sections shown in Figs. 7(b) and 7(c). The sharp velocity decline in all the pores of the first two cross sections indicates an important redistribution of fluid in adjacent pores. In addition, the particle accumulation leads to a significant decrease of velocity in all the pores. When there are more than 20 particles inside the clog the velocity inside the pores of each cross section becomes similar and as more particles accumulate it still decreases but much more slowly [Figs. 7(b)–7(e)]. These measurements confirm that the accumulation of the first 20 particles leads to an important decay of the pore flow velocities due to the closure of the different preferential flow paths that connect both ends of the clog. As all these paths are closed there is a redistribution of the flow such that the fluid is forced to flow through narrower pores, before leaving the clog, increasing the viscous dissipation and leading to a higher flow decline across the entire clog.

C. Clogging transition with 1.8-μm particles

The flow decline associated with the clogging transition is more complicated when the same pore is clogged by smaller particles like the 1.8-μm PMMA since more particles are involved in the clogging process. While most of the flow decline takes place when around 20 particles accumulate inside the pore for the 3-μm particles we need roughly the same number of objects with the 1.8-μm particles just to completely block the pore for the first time [Fig. 2(c)]. Thus, we suppose that there is a redistribution of flow and closure of low-resistance flow paths inside the growing deposit before the channel is effectively clogged since there is a sharp velocity decline during this process [Fig. 2(c)]. However, it is very challenging to observe such flow redistributions because it requires us to have access to the structure of the forming clog as particles deposit, as is seen in the 3-μm particles. Instead, we determine the internal structure of the clog once it is formed and does not grow anymore, utilizing confocal imaging and image analysis [27,28] to determine the flow conditions within it. Note, for this work we used a model filter with different dimensions from those employed in the work described above. In this case the filter had a rectangular cross section and was slightly wider (9 μm) and higher (11 μm), which leads to a lower confinement with the ratio W/D, where D is the particle size, being two times greater. We distinguish two zones in the clog when we look at the variations of particle volume fraction (PVF) with the clog length that likely correspond to the pore obstruction and the subsequent growth of the clog due to the accumulation of particles. The PVF first increases over a distance L equal to 7–8 μm that roughly corresponds to the width of the pore W [Fig. 8(a)], while for distance greater than L the PVF becomes constant at around 32% [Fig. 8(a)]. We found such an evolution of the PVF along the pore for other clogs formed under the same conditions (see Fig. 11 in the Appendix).

As the PVF increases, the number of pores between the particles also becomes greater with their median size decreasing until they become a bit smaller than the mean particle size at the end of the first zone [Figs. 8(a)–8(c)]. The decrease of the mean pore size leads to an increase of the local hydrodynamic resistance, likely corresponding to the sharp velocity decline up to the channel obstruction reported in Fig. 2(c). These results suggest that the channel is clogged at the cross section located at L since particles cannot flow through most of the pores of the deposit [Figs. 8(b) and 8(c)]. However, even when the PVF reaches its maximum and becomes constant its value is low enough to have one wide zone in all the cross sections along the clog, a zone wide enough to let particles flow through it [Fig. 9(a)] and inside which, fluid flows faster than in the other pores [Fig. 9(b)]. It turns out that these wide zones are not directly connected to each other, between adjacent cross sections, i.e., they are not located at the same position in each cross section, which ensures that there is no continuous path that the particles can follow to be transported across the growing clog [Fig. 9(a)]. Therefore, the clogging process for the 1.8-μm particles does not correspond to the complete obstruction of a thin cross section of the channel, as it is the case for the 3-μm particles, but rather to the partial fouling of the channel that spreads over a distance $L \approx W$, thus corresponding to the clog head. This partial fouling leads to the formation of three to four paths through which 50% of the fluid flows [Fig. 8(d)]. The spatial heterogeneities in the head of the clogs likely come

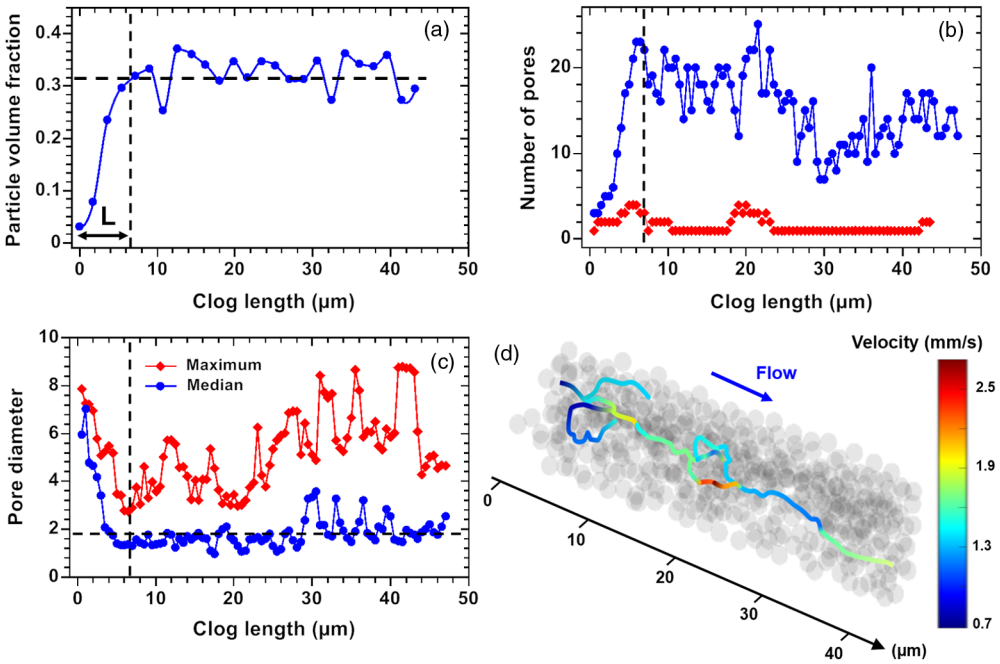

FIG. 8. (a) Variation of particle volume fraction inside the clog along the length of the clog, L_{clog}. The length L, equal to 6.5 μm, is the distance over which the particle volume fraction first increases, corresponding to the progressive obstruction of the pore until its complete clogging. The dashed line corresponds to the mean value of the volume fraction equal to 0.32. (b) Variation of the number of pores within the clog, in successive cross sections separated by 0.5 μm, through which all the fluid (top curve) or half of it (bottom curve) flows. (c) Evolution of the median diameter of the pores formed by particle accumulation and that of the widest pore in cross sections every 0.5 μm along the channel. (d) Three-dimensional flow paths inside the clog through which half the fluid flows.

from their composite nature, since they are systematically composed of a mixtures of aggregates, with various shapes and sizes, and spherical particles [21,22]. In the second part of the clog, for a clog length roughly equal to W, corresponding to the zone where particles start accumulating, the structure of the clog is also heterogeneous with noticeable fluctuations in the number of pores and also in their mean size [Figs. 8(b) and 8(c) and Fig. 9(a)]. As a consequence, the flow in this part of the clog is heterogeneous with 50% of the fluid that flows mainly through one wide path while the other 50% flows through 10 up to 15 narrower pores [Figs. 8(b)–8(d) and Fig. 9(b), images 10–40]. On average, this repartition of the flow between the pores remains the same all along the clog. We can consider that the permeability of the clog is constant and thus we have a Darcy flow through the clog, the flow rate decline being directly linked to the length of the clog, as already observed in a similar experiment [24]. The formation of this second part of the clog corresponds to the slowest velocity decline in Fig. 2 [Fig. 2(c), from time greater than 4 min].

We can perform numerical simulations of the flow across the clog, similar to what we did for the 3-μm particles even though we do not know how the 1.8-μm particles accumulated. However, since we have the precise position of each particle within the clog and if we suppose that there is no rearrangement during the clog formation, we are able to reconstruct the whole clog through successive steps. At each step we add a few particles to the clog and we determine the flow condition though the entire clog. However, we do not know when each particle deposits so we decided to add ten particles at the rear of the clog at each step, corresponding on average to a 1.4-μm-thick cross section. The particles that belong to each added section are chosen such that their distances from

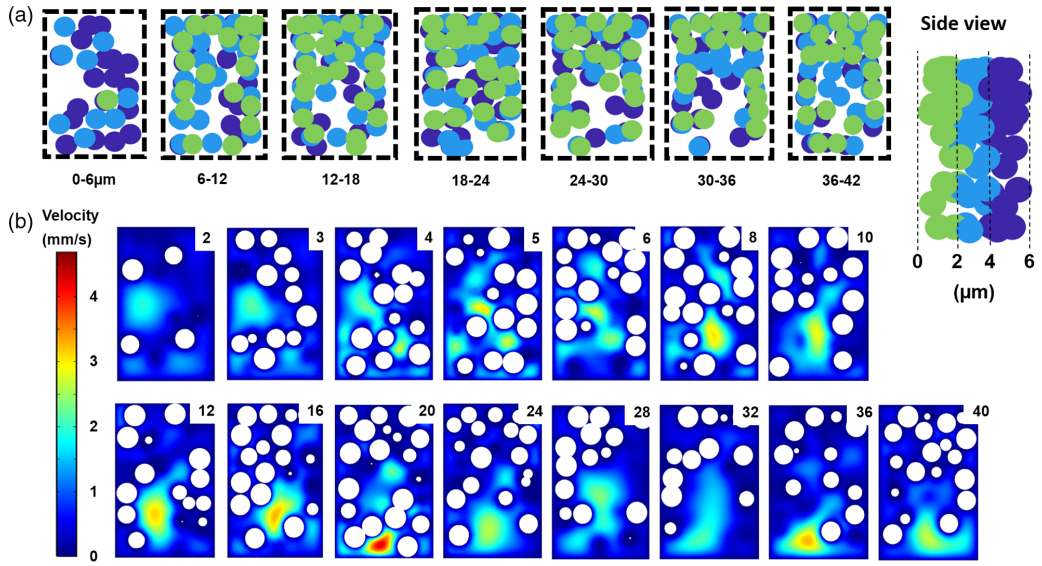

FIG. 9. (a) A 6-μm-thick cross section of the clog starting from the clog head. The side view on the right corner shows the color code associated with the three cross sections that compose the wider cross sections. (b) Fluid velocity map in a different cross section of the clogged pore. The position of the cross section in microns from the entrance of the clog is reported in the top right corner.

the rear of the clog are the smallest. Therefore, we cannot determine accurately the evolution of fluid velocity in the pores between the particles as they deposit, as we did for the 3-μm particles in Fig. 5, but we still have access to the variations of the fluid velocity across the growing clog (Fig. 10). We again found that there are three contributions to the flow decline. The obstruction of the pores requires the capture of about 40 particles, which pile up nonuniformly along a 7-μm zone which corresponds to the clog head. In a second zone, 8–9 μm further inside the clog, there is presumably an important redistribution of the flow paths which has a slightly smaller contribution to the flow drop than the clog head. Finally, 16 μm from the very head of the clog, we obtain a Darcy-like flow with the fluid velocity being inversely proportional to the clog length (Fig. 10, inset), even though the flow is rather heterogeneous [Figs. 8(b) and 8(d)].

IV. CONCLUSION

We have determined the variation of the flow conditions corresponding to the clogging of a single straight pore (channel) by colloidal particles, followed by the accumulation of particles at the rear of the clog. We have shown that there are three main contributions to the flow decline. Firstly, few particles accumulate and block a cross section of the channel, which leads to a narrowing of the cross section of the channel through which the fluid flows. During this obstruction process the fluid is progressively forced to flow through the pores formed by the accumulation of the particles, which become more and more narrow. When the channel is completely clogged no particles can flow through it and the mean pore size has become smaller than the particle diameter. Such a reduction of the size of the flow cross section contributes significantly to the overall flow decline. As expected, the smaller the particles the greater the decline in flow as the pores of the clog are smaller [29]. Thereafter, there is a sieving process of the incoming particles. As these accumulate there is a progressive closure of low-resistance flow paths that connect the head and the rear of the growing clog. This limited growth of the clog also contributes significantly to the flow decline. This process takes place when the length of the clog is still small, around 10 μm, irrespective of the particle

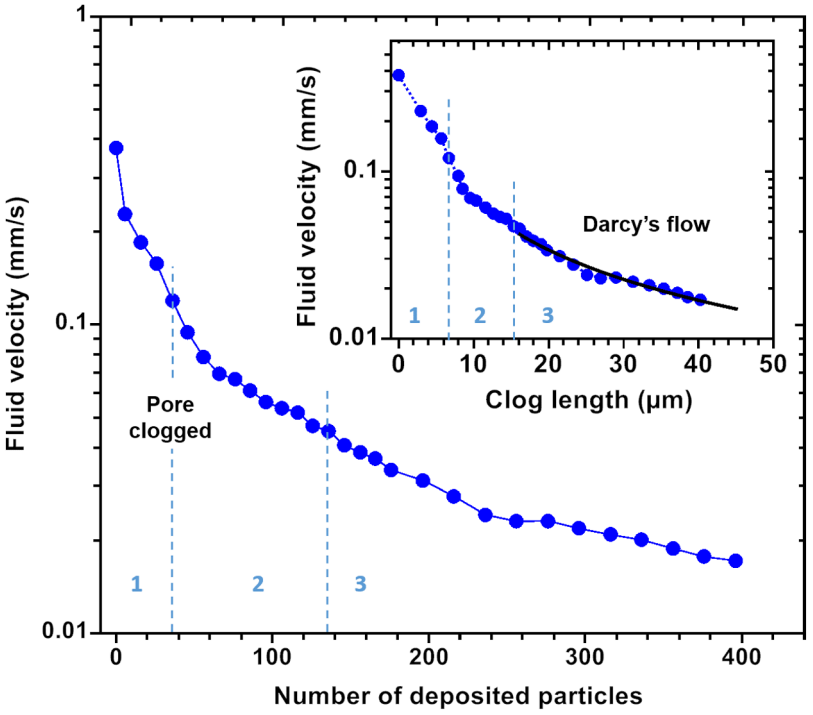

FIG. 10. Variation of the average fluid velocity through the clog as 1.8-μm PMMA particles accumulate in a numerical simulation of the clog formation and the flow within it. The average fluid velocity in the channel without any particle deposited corresponds to the first point of the graph. The pore is clogged when 38 particles are deposited, the end of this process being outlined by the vertical dashed line. The beginning of the part of the clog in which there is a Darcy flow is indicated by the vertical dotted line, when 138 particles have accumulated in the channel. (Inset) Evolution of the fluid velocity with the clog length. The three stages that contribute to the flow decline are separated by two dashed lines.

size and which corresponds to the width of the pore. The amplitude of the flow decline associated with the formation of these layers is highly dependent on the sizes and shapes of the particles that form the clog. The loss of some preferential flow paths forces the fluid to flow through more pores that are also narrower, resulting in a higher viscous dissipation and thus to lower flow conditions across the clog. More work has to be performed to better quantify the relationship between the flow redistribution and the flow drop in this second step. In the third and final step, for clog lengths greater than W-$2W$, depending on the particle diameter, the flow decline is only due to the increase of the clog length. The fluid velocity is inversely proportional to the clog length, indicating that we have a Darcy-like flow through this part of the clog, which thus has a constant permeability even though the flow can be quite heterogeneous with a broad distribution of the pore sizes formed by the accumulated particles. Therefore, when straight pores are clogged by colloidal particles, with a ratio $2 < W/D < 10$, we can safely consider that there is a Darcy flow across the particle accumulation from a distance equal to $2W$ from the entrance of the clog. The contribution of this third step to the hydrodynamic resistance of the entire clog is much less important than the first two even for long clogs, which is confirmed by our detailed analysis of the flow conditions within the clog thanks to numerical simulations for two particle sizes. Consequently, these results show unambiguously that the early dynamics of pore clogging has a greater impact on the flow decline than the subsequent growth of the clog. We think that our results can be applied to real pores, like those that compose filtration membranes or are found in natural porous environments, even though these do not look

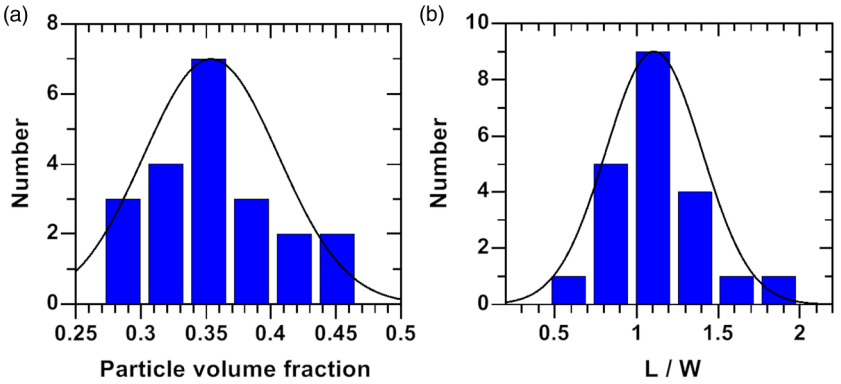

FIG. 11. (a) Variation of the particle volume fraction for 20 clogs formed with 1.8-μm PMMA particles in the same geometry with a width and a height of 9 and 11 μm, respectively. (b) Histogram of the size of the head of the clog, L, scaled by the width W of the pore.

like simple straight channels. As expected, there could be large variations in the amplitude of the flow decline for real pores whose size and shape of cross section are not constant. An interesting extension of this work would be to study the flow inside a growing clog when the flow rate rather than the pressure is fixed. In this case, there will be a great challenge in measuring the temporal variations of the pressure at the pore scale linked to the particle deposition. We also expect that the structure of the clogs partly composed of aggregates will be different, as well as its composition and clogging time. Indeed, the available cross section of the pore available for fluid flow will decrease as the deposits grow, which will require an increase in the pressure in order to keep the flow rate constant. Therefore, erosion or destabilization of the deposit may occur more often [30]. In such a case larger aggregates will be more involved in the clogging process since they are more stable under flow, i.e., they are less likely to be detached by the flow than smaller aggregates [22].

ACKNOWLEDGMENTS

We acknowledge the support of the Agence Nationale de la Recherche (ANR) (Grant No. ANR-12-JS09-0003) and the CNES (Collmat).

APPENDIX

We analyzed the structure of twenty clogs formed in the same conditions. We focus on the value of particle volume fraction at the rear of the clog and also on the length of the head of the clog.

[1] W. R. Bowen, J. I. Calvo, and A. Hernández, Steps of membrane blocking in flux decline during protein microfiltration, J. Membr. Sci. **101**, 153 (1995).

[2] A. Lee, K. Sudau, K. H. Ahn, S. J. Lee, and N. Willenbacher, Optimization of experimental parameters to suppress nozzle clogging in inkjet printing, Ind. Eng. Chem. Res. **51**, 13195 (2012).

[3] S. Bounoua, S. Tomas, J. Labille, B. Molle, J. Granier, P. Haldenwang, and S. N. Izzati, Understanding physical clogging in drip irrigation: In situ, in-lab and numerical approaches, Irrig. Sci. **34**, 327 (2016).

[4] Z. B. Sendekie and P. Bacchin, Colloidal jamming dynamics in microchannel bottlenecks, Langmuir **32**, 1478 (2016).

[5] L. Sicignano, G. Tomaiuolo, A. Perazzo, S. P. Nolan, P. L. Maffettone, and S. Guido, The effect of shear flow on microreactor clogging, Chem. Eng. J. **341**, 639 (2018).

[6] R. L. Hartman, J. R. Naber, N. Zaborenko, S. L. Buchwald, and K. F. Jensen, Overcoming the challenges of solid bridging and constriction during Pd-catalyzed C-N bond formation in microreactors, Org. Process Res. Dev. **14**, 1347 (2010).
[7] R. Blazejewski and S. Murat-Blazejewska, Soil clogging phenomena in constructed wetlands with subsurface flow, Water Sci. Technol. **35**, 183 (1997).
[8] C. Mikutta, F. Lang, and M. Kaupenjohann, Soil organic matter clogs mineral pores, Soil Sci. Soc. Am. J. **68**, 1853 (2004).
[9] W. Zhang, X. Tang, N. Weisbrod, and Z. Guan, A review of colloid transport in fractured rocks, J. Mt. Sci. **9**, 770 (2012).
[10] M. Manga, I. Beresnev, E. E. Brodsky, J. E. Elkhoury, D. Elsworth, S. E. Ingebritsen, D. C. Mays, and C.-Y. Wang, Changes in permeability caused by transient stresses: Field observations, experiments, and mechanisms, Rev. Geophys. **50**, 2011RG000382 (2012).
[11] T. Candela, E. E. Brodsky, C. Marone, and D. Elsworth, Laboratory evidence for particle mobilization as a mechanism for permeability enhancement via dynamic stressing, Earth Planet. Sci. Lett. **392**, 279 (2014).
[12] S. Veerapaneni and M. R. Wiesner, Deposit morphology and head loss development in porous media, Environ. Sci. Technol. **31**, 2738 (1997).
[13] D. C. Mays and J. R. Hunt, Hydrodynamic and chemical factors in clogging by montmorillonite in porous media, Environ. Sci. Technol. **41**, 5666 (2007).
[14] N. Bizmark, J. Schneider, R. D. Priestley, and S. S. Datta, Multiscale dynamics of colloidal deposition and erosion in porous media, Sci. Adv. **6**, eabc2530 (2020).
[15] B. Dersoir, A. B. Schofield, and H. Tabuteau, Clogging transition induced by self filtration in a slit pore, Soft Matter **13**, 2054 (2017).
[16] B. Dersoir, M. R. de S. Vincent, M. Abkarian, and H. Tabuteau, Clogging of a single pore by colloidal particles, Microfluid. Nanofluidics **19**, 953 (2015).
[17] M. Auset and A. A. Keller, Pore-scale processes that control dispersion of colloids in saturated porous media, Water Resour. Res. **40**, W03503 (2004).
[18] M. Auset and A. A. Keller, Pore-scale visualization of colloid straining and filtration in saturated porous media using micromodels, Water Resour. Res. **42**, 2005WR004639 (2006).
[19] A. Marin, H. Lhuissier, M. Rossi, and C. J. Kähler, Clogging in constricted suspension flows, Phys. Rev. E **97**, 021102(R) (2018).
[20] A. Sauret, E. C. Barney, A. Perro, E. Villermaux, H. A. Stone, and E. Dressaire, Clogging by sieving in microchannels: Application to the detection of contaminants in colloidal suspensions, Appl. Phys. Lett. **105**, 074101 (2014).
[21] N. Delouche, A. B. Schofield, and H. Tabuteau, Dynamics of progressive pore clogging by colloidal aggregates, Soft Matter **16**, 9899 (2020).
[22] N. Delouche, J. M. van Doorn, T. E. Kodger, A. B. Schofield, J. Sprakel, and H. Tabuteau, The contribution of colloidal aggregates to the clogging dynamics at the pore scale, J. Membr. Sci. **635**, 119509 (2021).
[23] C. Duchêne, V. Filipe, S. Huille, and A. Lindner, Clogging of microfluidic constrictions by monoclonal antibody aggregates: Role of aggregate shape and deformability, Soft Matter **16**, 921 (2020).
[24] A. Sauret, K. Somszor, E. Villermaux, and E. Dressaire, Growth of clogs in parallel microchannels, Phys. Rev. Fluids **3**, 104301 (2018).
[25] J. Lohaus, F. Stockmeier, P. Surray, J. Lölsberg, and M. Wessling, What are the microscopic events during membrane backwashing?, J. Membr. Sci. **602**, 117886 (2020).
[26] K. Alim, S. Parsa, D. A. Weitz, and M. P. Brenner, Local Pore Size Correlations Determine Flow Distributions in Porous Media, Phys. Rev. Lett. **119**, 144501 (2017).
[27] M. C. Jenkins and S. U. Egelhaaf, Confocal microscopy of colloidal particles: Towards reliable, optimum coordinates, Adv. Colloid Interface Sci. **136**, 65 (2008).
[28] B. Dersoir, A. B. Schofield, M. Robert de Saint Vincent, and H. Tabuteau, Dynamics of pore fouling by colloidal particles at the particle level, J. Membr. Sci. **573**, 411 (2019).

[29] S. Raha, K. C. Khilar, P. C. Kapur, and Pradip, Regularities in pressure filtration of fine and colloidal suspensions, Int. J. Miner. Process. **84**, 348 (2007).

[30] B. Dincau, C. Tang, E. Dressaire, and A. Sauret, Clog mitigation in a microfluidic array via pulsatile flows, Soft Matter **18**, 1767 (2022).